Parallelized Unstructured-Grid Finite Volume Method for Modeling Radiative Heat Transfer

Gunhong Kim, Seokgwon Kim, Yongmo Kim*
Department of Mechanical Engineering, Hanyang University, Seoul 133-791, Korea

In this work, we developed an accurate and efficient radiative finite volume method applicable for the complex 2D planar and 3D geometries using an unstructured-grid finite volume method. The present numerical model has fully been validated by several benchmark cases including the radiative heat transfer in quadrilateral enclosure with isothermal medium, tetrahedral enclosure, a three-dimensional idealized furnace, as well as convection-coupled radiative heat transfer in a square enclosure. The numerical results for all cases are well agreed with the previous results. Special emphasis is given to the parallelization of the unstructured-grid radiative FVM using the domain decomposition approach. Numerical results indicate that the present parallel unstructured-grid FVM has the good performance in terms of accuracy, geometric flexibility, and computational efficiency.

Key Words : Radiative Heat Transfer, Unstructured-Grid Finite Volume Method, Parallel Algorithm

1. Introduction

The modeling of radiative heat transfer is important in many engineering and industrial applications, such as furnaces and heat exchanger of semiconductors. Recently, the finite-volume method (FVM) has been emerged as the most viable and robust tool for analyzing the radiative heat transfer, due to its simplicity and ability to handle complex geometries.

The radiative FVM developed by Raithby and Chui (1990) possesses several attractive features for radiation modeling. The formulation of this approach is based on the same computational mesh employed for the fluid flow and combustion calculations. Moreover, this model inherently ensures the global conservation of radiant energy, because the inflow and outflow of radiant energy across control-volume faces are balanced with attenuation and augmentation of radiant energy within a control volume and a control angle. In this FVM, the radiative transfer equation (RTE) is solved for a discrete number of finite solid angles and the RTE for each direction is integrated over the control volume and discretized by the procedures similar to those for fluid flow. Another merit could be the flexibility and capability to handle the arbitrary coordinate and control angle (Chai et al., 1995). After Raithby and Chui proposed the FVM for radiation, numerous computational studies have been carried out for planar, 3D geometry, and axisymmetry by using the structured and unstructured grid (Back et al., 1998 ; Murthy and Mathur, 1998a, 1998b ; Raithby et al., 1999 ; Liu et al., 2000).

In many high-temperature systems, radiative heat transfer is usually strongly coupled with fluid dynamics and an accurate modeling of these problems requires a simultaneous solution of the RTE and the fluid dynamics equations (Chui et al., 1993). Thus, the radiative transfer model

* Corresponding Author,
E-mail : ymkim@hanyang.ac.kr
TEL : +82-2-2290-0428; **FAX** : +82-2-2297-0339
Department of Mechanical Engineering, Hanyang University, Seoul 133-791, Korea. (Manuscript **Received** August 6, 2004; **Revised** February 5, 2005)

must be computationally efficient for coupling the other submodels and numerical procedure used for the RTE must be compatible with the transport equations for other physical processes. In modeling the radiation process of the computationally intensive thermal flow problems, it is recognized that the parallel processing is an essential element to drastically reduce the time required for numerical solution (Goncalves and Coelho, 1997; Liu et al., 1999; Tal et al., 2003). Several approaches to parallelization of radiative transfer problems are available. These approaches include angular decomposition parallelization (ADP) and spatial-domain decomposition parallelization (DDP), which are natural choices especially in many practical situations. Compared to the ADP, the DDP has the more attractive feature, since this parallel strategy is widely used in parallel computational fluid dynamics codes. Another reason to prefer the DDP is that the number of ordinates is usually moderate but the number of spatial cells can be much larger in realistic problems. Thus the DDP is leading to the much better work balance and diminished communications overhead if the spatial grid is decomposed. Furthermore, an ADP algorithm in distributed-memory machines requires the storage of all variables at each cell and this results in a large memory requirement that could be too excessive for some machines.

In the unstructured-grid system, the use of parallel algorithms for the fluid transport and radiation transport would significantly complicate the overall parallel algorithm and increase the communication overhead. However, for very complicated systems, the labor required for grid generation is too time consuming, and it is often the largest portion of the entire effort for flow analyses. Currently, in the fluid-flow simulation, the unstructured-grid techniques have gained the wide popularity mainly due to the simplicity of grid generation and the flexibility of mesh adaptation in the complex flow regions. Because of its obvious advantages, the unstructured methods have also begun to receive attention in the community of radiative heat transfer previously.

This study has mainly motivated to develop an accurate, efficient and stable unstructured-grid FVM for numerically analyzing the flow-coupled radiative heat transfer of the complex multi-dimensional thermal systems. In order to drastically reduce the computing time in dealing with the large-scale practical problems, a spatial domain-based parallel algorithm has been devised for the unstructured-grid radiative FVM in a distributed computing environment. Moreover, in the numerical simulation of arbitrary-shaped radiation problems, the present unstructured-grid FVM adopts the pixelation procedures (Murthy and Mathur, 1998a) to treat the control angle overlapping problem which is inevitably occurring in computation for complex unstructured-grid systems.

The present numerical approach has fully been validated against the well-known benchmark cases. The validation cases include the radiative heat transfer in quadrilateral enclosure with isothermal medium, tetrahedral enclosure, a three-dimensional idealized furnace, as well as convection-coupled radiative heat transfer in a square enclosure. Numerical results obtained in this study confirm that the present parallel unstructured-grid FVM has the satisfactory capability for analyzing the flow-coupled radiative heat transfer of the geometrically and physically complex thermal systems in terms of accuracy, geometric flexibility, and computational efficiency.

2. Mathematical Formulation

2.1 Radiative transfer equation

The RTE for a gray absorbing, emitting, and scattering gas in a specified direction $\boldsymbol{s}$ at any position $\boldsymbol{r}$ may be written as (Modest, 1993)

$$\frac{dI(\boldsymbol{r}, \boldsymbol{s})}{ds} = -[\kappa(\boldsymbol{r}) + \sigma(\boldsymbol{r})] I(\boldsymbol{r}, \boldsymbol{s}) + \kappa(\boldsymbol{r}) I_b(\boldsymbol{r}) + \frac{\sigma(\mathbf{r})}{4\pi} \int_{4\pi} I(\boldsymbol{r}, \boldsymbol{s}') \Phi(\boldsymbol{s}', \boldsymbol{s}) d\Omega' \tag{1}$$

where $I(\boldsymbol{r}, \boldsymbol{s})$ is the radiative intensity, which is a function of position and direction; $I_b(\boldsymbol{r})$ is the black-body radiative intensity at the temperature of the medium; κ and σ are the absorption and

scattering coefficients, respectively; $\Phi(s', s)$ and is the scattering-phase function from the incoming s' direction to the outgoing direction s. In the Cartesian coordinates (x, y, z), the spatial derivative term in Eq. (1) can be written as

$$\frac{dI}{ds}=\mu\frac{dI}{dx}+\eta\frac{\partial I}{\partial y}+(idim-2)\,\xi\frac{\partial I}{\partial z} \quad (2)$$

where μ, η, and ξ are the direction cosines along the Cartesian coordinates x, y, and z directions, *idim* denotes the dimensionality of the problem and is equal to 2 for a 2D planar geometry and 3 for a 3D geometry.

All boundaries are assumed to be gray-diffuse. Under this assumption, the wall bounding the medium emits and reflects diffusely. The wall boundary intensity I_W for all outgoing direction $(s\cdot n<0)$ is given by

$$I_W=\varepsilon I_b(r_w)+\frac{1-\varepsilon}{\pi}\int_{s\cdot n>0} I(r_w, s)\,s\cdot n\,d\Omega \quad (3)$$

where ε is the wall emissivity and the unit vector n is the surface normal pointing out of the domain.

2.2 Energy equation

For problems in which the heat transfer due to radiation is considered, it is necessary to solve the energy equation including the additional source term of the radiative heat transfer. If, for simplicity, the specific heat capacities are all equal and constant, the pressure is constant, the energy equation of temperature form becomes

$$\rho c_p\frac{\partial T}{\partial t}+\rho c_p v\cdot\Delta T =\nabla\cdot(\lambda\nabla T)+S_h+\nabla\cdot q_{Rad} \quad (4)$$

Here, S_h contains the source of energy (i.e. the heat release due to combustion) and $\nabla\cdot q_{Rad}$ is the additional source of radiative energy loss. This radiative energy loss term for a gray absorbing, emitting, and scattering gas will be obtained from the RTE and may be written as

$$\nabla\cdot q_{Rad}=\kappa(r)\int_{4\pi}[I(r, s)-I_b(r)]\,d\Omega \quad (5)$$

3. Unstructured-Grid Finite Volume Method

3.1 Discretization

The RTE, Eq. (1) involves not only spatial differentiation but also the angular integration over the solid angle ω. To solve this equation numerically, both spatial domain and angular domain must be discretized at first. In this study, an unstructured control volume method is used to discretize the spatial domain. The computational domain is identified and divided into many volume cells as seen in Fig. 1(a). The cell types vary from triangular to quadrilateral for 2D problems and tetrahedral, prism, pyramid, to hexahedral for 3D problems. The cell type in each problem can be single or mixed. All

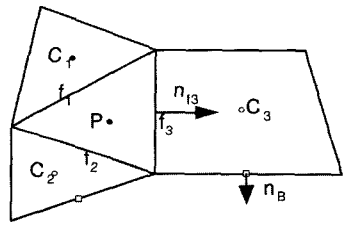

• Infield cell
° Near-boundary cell
□ Boundary ghost cell

(a) Cell-center control volume for 2D unstructured grids

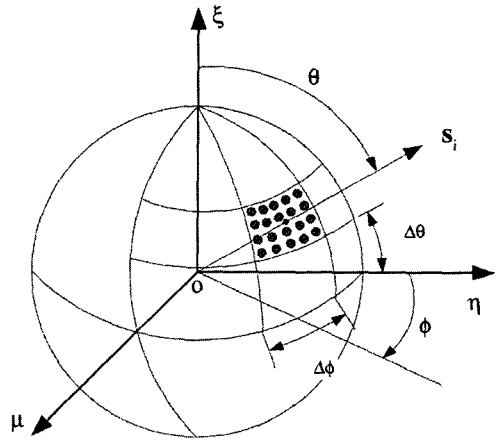

(b) Angular discretization

Fig. 1 Discretization of unstructured finite volume method for RTE

unknown variables are stored at cell centers.

Discretization of the angular domain is similar to that for the spatial domain. The angular space 4π at any spatial location is discretized into discrete, non-overlapping solid angles ω_i, the centroids of which are denoted by the direction vector $\boldsymbol{s}_i$. In this study, we use the azimuthal discretization stategy with the FVM. As shown in Fig. 1(b) for the Cartesian coordinate system, all extents are given equally by $\Delta\theta$ and $\Delta\phi$, respectively.

3.2 Control volume balance

For each discrete direction si the discretized RTE can be obtained by integrating Eq. (1) over a control volume P in Figure 1(a) and a solid angle ω_i to yield

$$\sum_{f=1}^{N_P} I_f^i A_f D_f^i = \left[-(\kappa+\sigma) I^i + \kappa I_b + \frac{\sigma}{4\pi}\sum_{j=1}^{M}\omega_j \Phi^{ij} I^j\right]_p \omega_i \Delta V_p \tag{6}$$

Here, N_P is the total face number for the cell P, A_f is the f-th face area, D_{fi} is the product of the unit normal vector at the face and the intensity direction $\boldsymbol{s}_i$. The radiative intensities along the direction $\boldsymbol{s}_i$ and $\boldsymbol{s}_j$ are I_i and I_j, respectively, and ω_i is the solid angle associated with the direction $\boldsymbol{s}_i$, ΔV_P is the volume of the cell P, M is the total number of discrete directions.

To close Eq. (6) and to incorporate with the cell-center unstructured finite volume solver, relations are needed between the intensities on the cell faces and the cell center ones. One popular closure scheme for complicated geometries or grid systems is based on the step scheme, which sets the downstream face intensity equal to the upstream cell-center value (Chai et al., 1995). Applying this scheme to the cell P in Fig. 1(a), typical relations between face-intensities and cell-center values are as follows

$$I_f^i = \max(A_f D_f^i, 0) I_P^i - \max(-A_f D_f^i, 0) I_{C_f}^i \tag{7}$$

where C_f is the neighbor cell of the cell P and the f-th face is the common face between P and C_f, and $I_{C_f}^i$ denotes the intensity at the cell C_f. Then, the final discretized form of Eq. (6) becomes

$$\left[\sum_{f=1}^{N_P}\max(A_f D_f^i, 0) + (\kappa+\sigma)\omega_i \Delta V_P\right] I_P^i = \sum_{j=1}^{N_P}\max(-A_f D_f^i, 0) I_{C_f}^i + \left[\kappa I_b + \frac{\sigma}{4\pi}\sum_{j=1}^{M}\right]_P \omega_i \Delta V_P \tag{8}$$

3.3 Treatment of control angle overhang

In a general unstructured grid approach, the inevitable control-angle overhang happens not only at boundaries but also at the interior. To address control-angle overhang, in this study, the recipes of Murthy and Mathur (1998a) are adopted. If the direction i exhibits overhang at the face f, the incoming and outgoing portions of the solid angle are differenced differently. To obtain the incoming and outgoing face intensities, Eq. (7) is written as

$$I_f^i = \alpha_{\text{out}} I_P^i + \alpha_{\text{in}} I_{C_f}^i \tag{9}$$

where

$$\alpha_{\text{out}} = A_f \cdot \int_{\Delta\theta}\int_{\Delta\phi} \boldsymbol{s}\sin\theta d\theta\, d\phi,\ A_f \cdot \boldsymbol{s} > 0$$

$$\alpha_{in} = A_f \cdot \int_{\Delta\theta}\int_{\Delta\phi} \boldsymbol{s}\sin\theta d\theta\, d\phi,\ A_f \cdot \boldsymbol{s} \le 0$$

Therefore, the problem of computation of the overhang angles is to calculate the incoming and outgoing radiative fluxes with respect to the interested cell center. According to pixelating of Murthy and Mathur (1998a), the solid angle of interest is divided into $N_{\theta P} \times N_{\phi P}$ pixels and the incoming and outgoing radiative fluxes of overhang face are calculated by the computation over all pixels in the control angle. As mentioned by Murthy and Mathur (1998a), using this pixelating approach, control angle overhang can be computed up to the pixel resolution. In almost cases, computational load of pixelation may be minimized by pixelating only those control angles that exhibit overhang at boundaries without the sacrifice of accuracy.

3.4 Linear solver

The discretization procedure leads to a set of linear equations relating the value of radiative intensity of i-th discrete direction at the cell center to its cell neighbors:

$$a_P I_P^i = \sum_{nb} a_{nb} I_{nb}^i + b \tag{10}$$

Here, nb is the number of cell neighbors. The intensities associated with other discrete directions are included in the b term. In this work, a sequential iterative approach is adopted. The above discrete set of algebraic equations for each direction i is solved, looping through all the directions until convergence. The solver of the discretized equations is based on a Gauss-Seidel procedure.

3.5 Parallelization strategy of radiative heat transfer

Considering the parallelization strategy of the RTE, the spatial domain decomposition parallelization is very attractive for the solution of coupled reactive fluid flow/heat transfer problems, because the domain decomposition approach is usually employed in computational fluid dynamics. Therefore, the governing transport equations and the RTE can be parallelized in a similar fashion. In the spatial domain decomposition approach the computational domain is divided into a number of sub-domains equal to the number of processors. Although the sub-domains do not overlap, there is a buffer of halo points added to their boundaries, including the virtual boundaries, i.e., interfacial boundaries between neighboring processors. These halo points are needed because the radiation intensities at the cell centers are stored in an array, but the radiation intensities at cell faces are not. A plane of halo points is added to each sub-domain boundary to enable the exchange of data (radiation intensities) at the virtual boundaries between neighboring processors. More details of treatment of the virtual boundary to communicate the information have been well documented by Kang (2002).

4. Results and Discussion

4.1 Radiation in quadrilateral enclosure with isothermal medium

As the first test problem, the FVM is applied to analyze the radiative heat transfer in a quadrilateral enclosure with containing an absorbing-emitting medium maintained at a $T=T_h$. The vertices of the box, in counterclockwise, are (0, 0), (2.2, 0), (1.5, 1.2), and (0.5, 1.0). Figure 2(a) shows an irregular quadrilateral enclosure and all dimensions are in meters. The black walls are kept at 0 K and three absorption coefficients, 0.1, 1, and 10 m^{-1} are studied. The objective is to predict the dimensionless incoming radiative flux on the walls and to compare it with the exact solution, generated by means of a ray-tracing method (Baek et al., 1998). This problem has been used by Chai et al.(1995) and Baek et al. (1998) to validate their structured-grid finite volume scheme. Murthy and Mathur (1998a) also adopted this same problem to validate their finite volume scheme by using an unstructured-grid.

The initial results are obtained using a structured mesh of 10×10 quadrilateral control volumes and $N_\theta\times N_\phi$ of 2×8. This discretization is identical to that used by Chai et al.(1995).

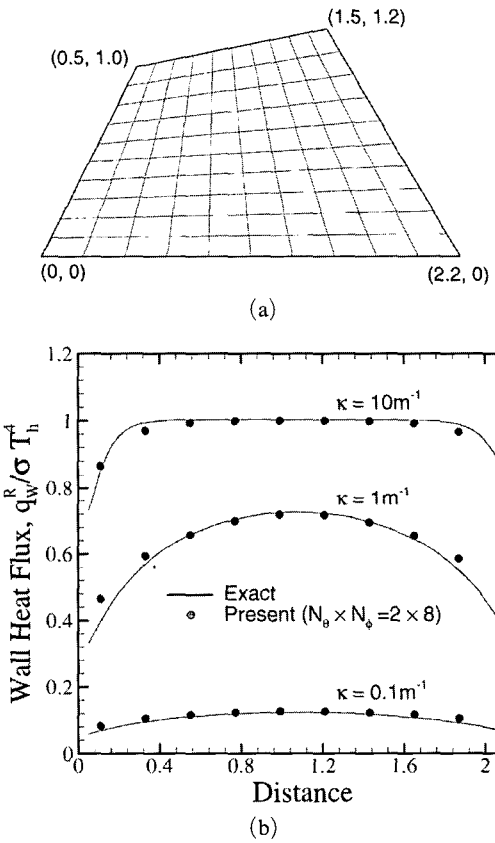

Fig. 2 A quadrilateral enclosure; (a) schematic and computational grid and (b) dimensionless heat fluxes on the bottom wall

The numerical scheme also defaults identically to theirs when the step scheme is used on a structured quadrilateral mesh. The dimensionless net heat fluxes at the bottom wall are shown in Fig. 2(b). Here distance, the length along the wall, is measured counterclockwise. It is seem that numerical results of various absorption coefficients are well agreed with the exact solutions. The departures from the exact solution are especially high at the corners.

Using finer structured quadrilateral meshes and a variety of angular discretization, the estimated errors for a bottom wall for $\kappa=1.0\ m^{-1}$ are tabulated in Table 1. The error is defined as

$$\text{Error}=\frac{1}{N}\sum_{n}\frac{|f_n-f_{n,exact}|}{|f_{n,exact}|} \tag{11}$$

where f_n is the computed value at point n, $f_{n,exact}$ is the exact value at the same point, and N is the total number of points. When the finer angular discretizations are used with a coarse structured mesh (10×10), the influence of the corners is not well captured by numerical solution. These numerical errors mainly stem from the spatial discretization error corresponding to the coarse mesh arrangement (10×10). By refining the spatial grid, numerical solution progressively approaches to the exact solution. Figure 3 shows an unstructured triangular mesh arrangement with 2684 cells. The corresponding predicted radiative flux of the bottom wall for $\kappa=1.0\ m^{-1}$ is displayed in Figure 4. These unstructured-grid results are quite close to those for the structured quadrilateral mesh. The numerical errors for 2×4, 2×8, 4×8, and 4×12 angular discretizations are 5.13, 2.88, 1.26, and 0.56%, respectively. These numerical results clearly indicate that, by utilizing finer quadrilateral or triangular grids and finer angular discretizations, the deviations from the exact value are considerably decreased. These trends are nearly identical to the previous nu-

Table 1 Estimated errors for quadrilateral enclosure for $\kappa=1.0\ m^{-1}$ *

Mesh	$N_\theta \times N_\phi$	Error, %
10×10	2×4	10.2
	2×8	4.54
	4×8	4.62
	4×12	3.64
20×20	2×4	8.69
	2×8	4.27
	4×8	2.65
	4×12	1.65
30×30	2×4	5.73
	2×8	3.44
	4×8	1.36
	4×12	0.79
40×40	2×4	5.00
	2×8	2.83
	4×8	1.22
	4×12	0.65

*Error in dimensionless heat flux for quadrilateral mesh.

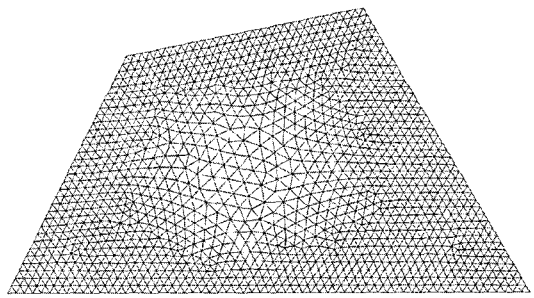

Fig. 3 Quadrilateral enclosure with isothermal medium, 2684 unstructured triangular mesh

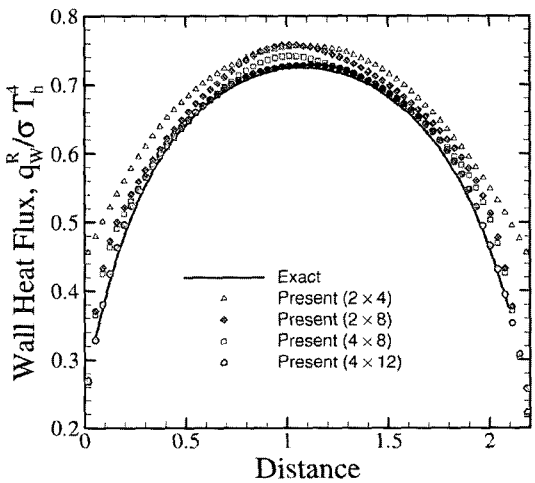

Fig. 4 Quadrilateral enclosure with isothermal medium, heat flux on the bottom wall for triangular mesh for $\kappa=1.0\ m^{-1}$

merical result (Murthy and Mathur, 1998a). If a higher-order spatial differencing scheme was used instead of the step scheme, the spatial error might be reduced more rapidly. However, it is widely recognized that the step scheme has its advantages against a high-order scheme because the step scheme is more stable and sufficiently accurate for a fine grid system. Moreover, the splendid adaptability of the unstructured-grid system could easily improve the solution quality of the step scheme by the local grid enrichment.

4.2 Radiation in tetrahedral enclosure

To demonstrate the predicative capability of the present unstructured-grid radiative FVM for three-dimensional complex geometries, we have chosen the radiation process of a tetrahedron of side L, which was numerically studied by Murthy and Mathur (1998a). The base of the tetrahedron lies on the x-y plane; the coordinates $(x/L, y/L, z/L)$ of the vertices are (0, 0, 0), (1, 0, 0), (0.5, 0.866, 0), and (0.5, 0.288, 0.817). The black walls are at $T=0$. The interior has a fixed temperature of $T=T_h$ and an optical thickness $\kappa L=1.0$. Figure 5(a) shows the unstructured-grid arrangement used in this study and 12,627 tetrahedral cells are used. The dimensionless incoming heat flux is computed along the face centerline including the side midpoint (0.75, 0.43, 0) and the top vertex (0.5, 0.288, 0.817) for different angular discretizations (6×6, and 8×8), with and without the boundary pixelation. In this example case, all numerical results using pixelation are based on $N_{\theta P}\times N_{\phi P}$ of 8×8.

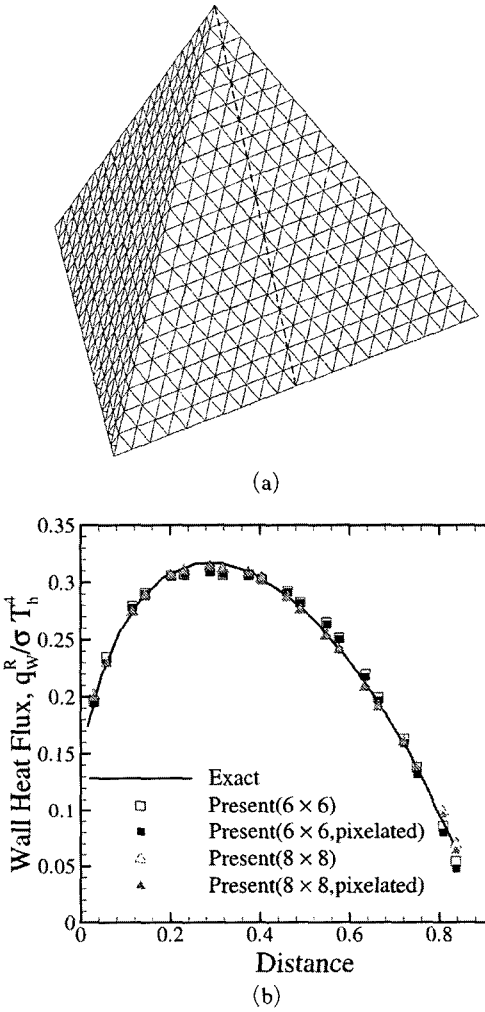

Fig. 5 Tetrahedral enclosure; the grid system and heat flux variation on face centerline

As shown in Fig. 5(b), the all predicted profiles of heat flux along the face centerline are seen to agree well with the exact solution.

Without boundary pixelation, the errors for 6×6 and 8×8 angular discretizations are 1.98 and 1.50%, respectively. With boundary pixelation, the corresponding errors are 1.95 and 1.18%, respectively. Numerical results indicate that, with the present fine grid system, the pixelation of boundary face marginally improves the numerical accuracy. Previously as stated by Murthy and Mathur (1998a), the use of the fine mesh reduces the spatial errors. For the finer mesh, Calculations using the boundary pixelation improves accuracy somewhat; however, it does not appear necessary for practical calculations.

4.3 Radiation in a three-dimensional idealized furnace

Next, in order to evaluate the modeling accuracy in the idealized furnace, the present approach has been applied to analyze the radiative heat transfer in three-dimensional rectangular combustor proposed by Menguc and Viskanta (1985). The model combustor contains an absorbing, emitting, and non-scattering medium with $\kappa=0.5\ \mathrm{m}^{-1}$. There exists a uniform internal heat

release rate of $S_h=5.0\,kW/m^3$ in the medium, which must satisfy the energy equation, Eq. (4). The temperature and emissivity of the hot wall at $z=0$ are 1,200 K and 0.85 while those of the cold wall at $z=4$ are 400 K and 0.70. At the all side walls, their temperature and emissivity are given as $T_W=900$ K and $\varepsilon_W=0.7$. Due to the internal heat source, this problem requires an iterative solution procedure for the energy equation, Eq. (4). Figure 6 shows the structure and unstructured grid arrangements for the three-dimensional idealized furnace. The structured grid has the 2,420 equal-spaced hexagons and the unstructured grid involves the 14,068 tetragons and 242 prisms. The angular domain is divided by 4×4 for the structured grid and by 6×6 for the unstructured grid, respectively. Because several results of by using different radiative models others (Menguc and Viskanta, 1985 ; Baek et al., 1988 ; Liu et al., 1996) have showed the similar predictions, in this work only zone solution was selected to test against the present results in Fig. 6 (Menguc and Viskanta, 1985).

In Fig. 7(a), the profiles of temperature are displayed along a line (x-axis direction) with $y=1.0$ m for three z locations. At all three z locations, numerical results for structured and unstructured grids are well agreed with the zone solution. In terms of the net radiative wall heat flux distribution along a line (x-axis direction) with $y=1.0$ m on the hot wall and cold wall, the agreement between the present results and the zone solution is quite good in Figure 7(b). These numerical results suggest that the present unstructured-grid approach has the capability to simulate the radiative heat transfer in the geome-

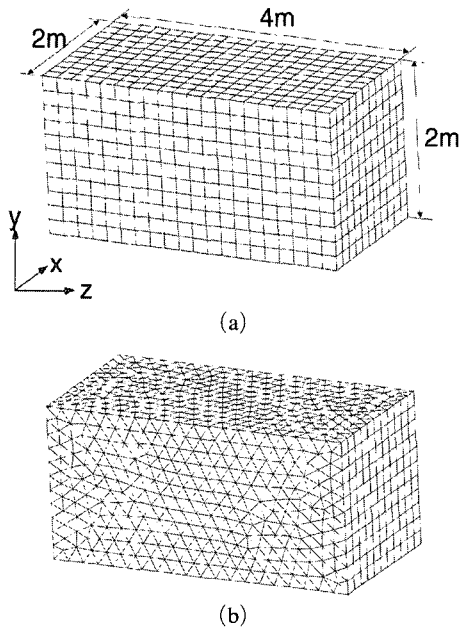

Fig. 6 3D idealized furnace ; (a) structured grid, (b) unstructured grid

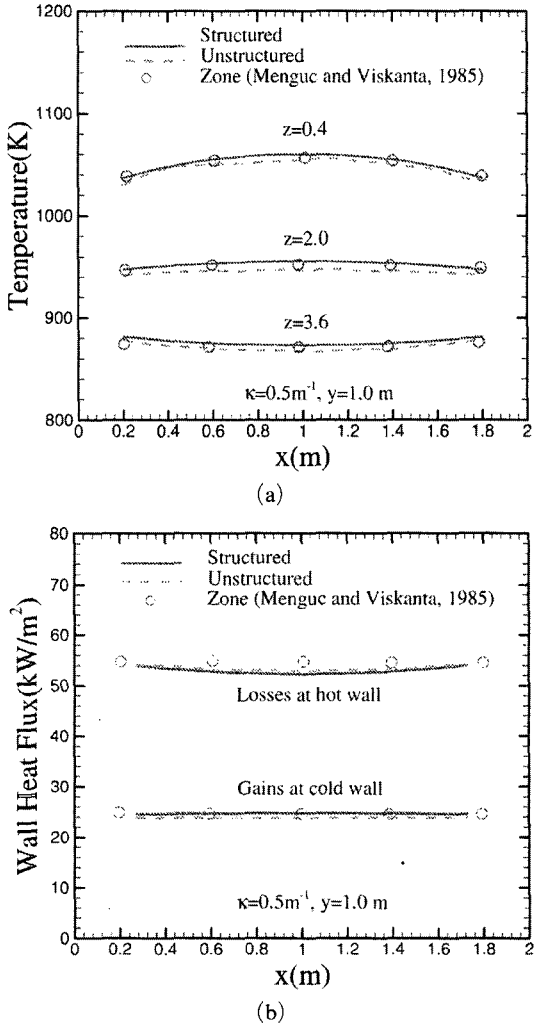

Fig. 7 Comparisons of (a) temperature distribution at different z locations and (b) radiative wall heat flux distributions at the hot and cold walls

trically and physically complex practical combustors.

4.4 Coupled radiation and natural convection in a square enclosure

The radiative heat transfer interacts strongly with convection in many practical thermal/fluid flow systems. In modeling convection-radiation interactions for a radiatively participating fluid, the efficient and accurate numerical model to be compatible with the CFD code is needed to predict the radiative transfer through the medium. To check the accuracy and numerical efficiency of the parallel unstructured-grid flow solver and radiative model, the present approach has been applied to analyze the coupling process of buoyancy and participating radiation in a square enclosure, which is showed schematically in Fig. 8.

This validation case was previously analyzed by Yucel et al.(1989), who used the SN discrete ordinates method. Murthy and Mathur (1998a) also validated the same problem by utilizing the unstructured radiative FVM. The fluid is Newtonian and incompressible. In order to limit the number of independent parameters, all physical properties are taken as constant except for the density. The flow is assumed to be laminar, steady, and two-dimensional. The working direction of gravity is downward. With these assumptions, the equations for the conservation of mass, momentum, and energy can be transformed to the corresponding equations of dimensionless form, which are illustrated well by Yucel et al.(1989). To consider the gravity effect, the Boussinesq approximation was used in the buoyancy terms to allow for the variation of density with temperature (Kim et al., 2002).

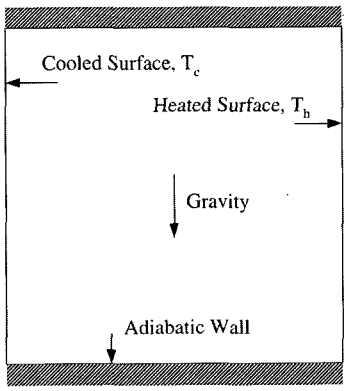

Fig. 8 Schematic representation of the physical system

In this square enclosure problem of Fig. 8, the left wall is at the cold-temperature condition, T_c and the right wall is at the hot-temperature condition, T_h. The top and bottom walls are insulated. The enclosure is filled with an absorbing and emitting gas. Computations are made for $Ra=5\times10^6$, $Pr=0.72$, $T_0/(T_h-T_c)=1.5$, $\kappa L=1.0$, and $Pl=\kappa L/(4\sigma T_0^3)=0.02$. Here T_0 is equal to $0.5(T_h+T_c)$, and L denotes the length of the side.

The mesh-arrangement used in all computations is the same as the 7666 triangular cells with 4-partitioned domains shown in Fig. 9(a). In

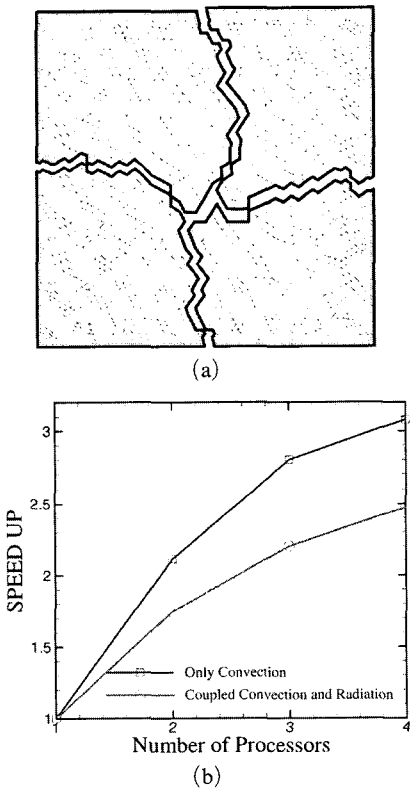

Fig. 9 Coupled convection and radiation in square enclosure, composed of 7666 cells totally; (a) 4-partitioned domains for parallel computation, (b) parallel efficiency of coupled convection and radiation

order to evaluate the parallel efficiency for analyzing the coupled convection and radiation, four computations are carried out for the different number of the parallel processors, which is same as the number of partitioned domains. In Fig. 9(b), in terms of the computational time, the parallel efficiencies are displayed to demonstrate the speed-up tendency with respect to the single-processor computation. It can be clearly seen that the parallel efficiency for analyzing only the convection process is much higher, compared to the convection-radiation coupled problem. This result could be explained by the message-passing load of the RTE, which is increased according to the number of solid angles, $N_\theta \times N_\phi$. Even if these results suggest that the computational load for analyzing radiation could be much higher especially for the fine grid system, it is obvious that the parallelization procedure with the enhanced optimization will considerably relax the computational load up to the certain degree. Regardless of number of processors, the present numerical results for all cases are nearly identical. Figure 10 shows a plot of the normalized u-velocity along the vertical centerline and the normalized v-velocity along the horizontal centerline, respectively. Numerical results indicate that the predicted velocity profiles are almost same as those obtained by Yucel et al.(1989) and Murthy and Mathur (1998a). However, there exist the marginally small differences between the present prediction and the previous computations. The marginal differences are considered to come mainly from using the different flow solver.

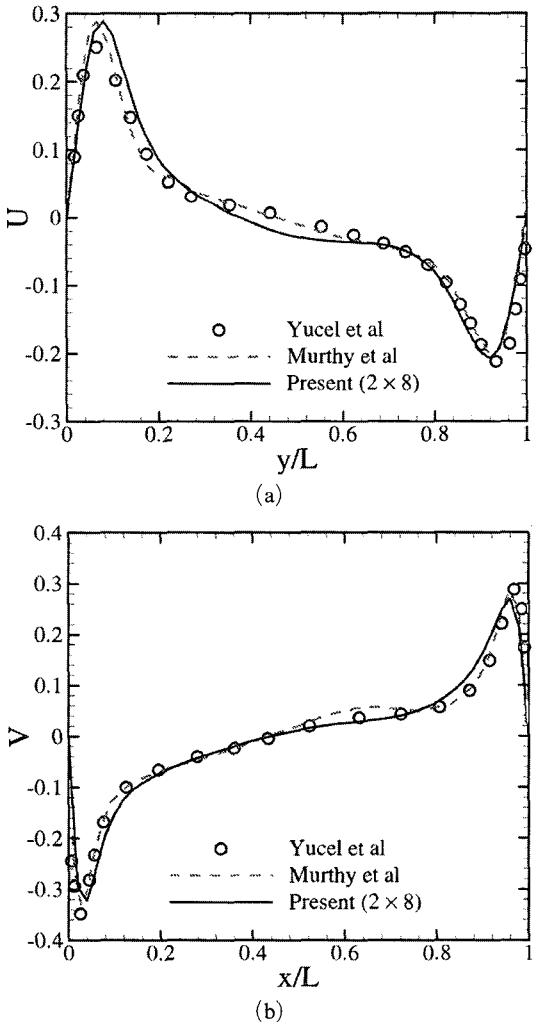

Fig. 10 (a) U-velocity along vertical centerline, (b) V-velocity along horizontal centerline

5. Conclusions

An unstructured finite volume method has been developed to numerically analyze the radiative heat transfer of the complex practical thermal-fluid flow systems. The validation cases include the radiative heat transfer in quadrilateral enclosure with isothermal medium, tetrahedral enclosures, a three-dimensional idealized furnace, as well as convection-coupled radiative heat transfer in a square enclosure. Based on numerical results obtained in this study, the following conclusion can be drawn.

(1) Numerical results for the quadrilateral enclosure with isothermal medium are well agreed with the exact solutions even if the departures from the exact solution are relatively high at the wall corners. By utilizing the refined grid and also fine angular discretization, the deviations at wall corners are considerably decreased.

(2) In case of the tetrahedral enclosure, the predicted profiles of heat flux along the face centerline are well agreed with the previous results. Numerical results also indicate that, with the fine

grid system, the pixelation of boundary face slightly improves the numerical accuracy.

(3) At all three z locations, numerical results for structured and unstructured grids are well agreed with the zone solution for a three-dimensional idealized furnace. In terms of the net radiative wall heat flux distribution at $y=1.0$ m, the agreement between the present results and the zone solution is quite good. These numerical results suggest that the present unstructured-grid approach has the capability to simulate the radiative heat transfer in the geometrically and physically complex practical combustors.

(4) The parallel efficiency for analyzing only the convection process is much higher, compared to the convection-radiation coupled problem. Even if the computational load for analyzing radiation could be higher especially for the fine grid system, it is expected that the parallelization procedure with the enhanced optimization could considerably reduce the computational load up to the certain degree. Regardless of number of processors, the present numerical results for all cases are nearly identical to the previous results.

Acknowledgments

This work was carried out as a part of the Next-Generation New Technology Development Program "Development of High Efficiency Gas Turbine/Fuel Cell Hybrid Power Generation System," which is supported by Ministry of Commerce, Industry and Energy, Korea.

References

Back, S. W., Kim, M. Y. and Kim, J. S., 1998, "Nonorthogonal Finite-Volume Solutions of Radiative Heat Transfer in a Three-Dimensional Enclosure," *Numerical Heat Transfer*, Vol. 34, Pt. B, pp. 419~437.

Chai, J. C., Parthasarathy, G., Lee, H. S. and Patankar, S. V., 1995, "Finite Volume Radiative Heat Transfer Procedure for Irregular Geometries," *J. Thermophys. Heat Transfer*, Vol. 9, No. 3, pp. 410~415.

Chui, E. H., Hughes, P. M. J. and Raithby, G. D., 1993, "Implementation of the Finite Volume Method for calculating Radiative Transfer in a Pulverized Fuel Flame," *Combust. Sci. and Tech.*, Vol. 92, pp. 225~242.

Goncalves, J. and Coelho, P. J., 1997, "Parallelization of the Discrete Ordinates Method," *Numerical Heat Transfer*, Vol. 32, Pt. B, pp. 151~173.

Kang, S. M., 2002, "Parallel Unstructured-Grid Finite-Volume Method for Non-reacting and Reacting Flows at All Speeds," Ph.D. Thesis, Hanyang University.

Kim, N. J., Lee, J. Y., Seo, T. B. and Kim, C. B., 2002, "Combined Convection and Radiation in a Tube with Circumferential Fins and Circular Disks," *KSME Int. J.*, Vol. 16, No. 12, pp. 1725~1732.

Liu, J., Shang, H. M. and Chen, Y. S., 1999, "Parallel Simulation of Radiative Heat Transfer Using and Unstructured Finite-Volume Method," *Numerical Heat Transfer*, Vol. 36, Pt. B, pp. 115~137.

Liu, J., Shang, H. M. and Chen, Y. S., 2000, "Development of an Unstructured Radiation Model Applicable for Two-Dimensional Planar, Axisymmetric, and Three-Dimensional Geometries," *J. Quant. Spectrosc. Radiat. Transfer*, Vol. 33, pp. 17~33.

Menguc, M. P. and Viskanta, R., 1985, "Radiative Transfer in Three-Dimensional Rectangular Enclosures Containing Inhomogeneous Anisotropically Scattering Media," *J. Quant. Spectrosc. Radiat. Transfer*, Vol. 33, No. 6, pp. 533~549.

Modest, M. F., 1993, Radiative Heat Transfer, Series in Mechanical Engineering, *McGraw-Hill*, New York.

Murthy, J. Y. and Mathur. S. R., 1998a, "A Finite Volume Method For Radiative Heat Transfer Using Unstructured Meshes," *AIAA*-98-0860, January.

Murthy, J. Y. and Mathur, S. R., 1998b, "Radiative heat Transfer in Axisymmetric Geometries using an Unstructured Finite-Volume Method," *Numerical Heat Transfer*, Vol. 33, Pt. B, pp. 397~416.

Raithby, G. D. and Chui, E. H., 1990, "A Finite-Volume Method for Predicting a Radiat

Heat Transfer in Enclosures with Participating Media," *J. Heat Transfer*, Vol. 112, pp. 415~423.

Raithby, G. D., 1999, "Discussion of the Finite-Volume Method for Radiation, and its Application using 3D Unstructured Meshes," *Numerical Heat Transfer*, Part B, 35 : pp. 389~405.

Tal. J.. Ben-Zvi. R. and Kribus. A.. 2003. "A High-Efficiency Parallel Solution of the Radiative Transfer Equation," *Numerical Heat Transfer*, Part B, 44 : pp. 295~308.

Yucel, A., Acharya, S. and Williams, M. L., 1989, "Natural Convection and Radiation in a Square Enclosure," *Numerical Heat Transfer*, Vol. 15, Part A, pp. 261~278.